International Journal of Biological Macromolecules 279 (2024) 135277

Contents lists available at ScienceDirect

International Journal of Biological Macromolecules

journal homepage: www.elsevier.com/locate/ijbiomac

Molecular basis of bacterial lectin recognition of eukaryotic glycans: The case of *Mycoplasma pneumoniae* and *Mycoplasma genitalium* cytoadhesins

Angela Marseglia [a,1], Maria Concetta Forgione [a,1], Marina Marcos-Silva [b], Cristina Di Carluccio [a], Yoshiyuki Manabe [c], David Vizarraga [d], Ferran Nieto-Fabregat [a], Maria Pia Lenza [a,g], Koichi Fukase [c], Antonio Molinaro [a,c], Oscar Q. Pich [b,e], David Aparicio [d,f], Alba Silipo [a,c], Roberta Marchetti [a,*]

[a] *Department of Chemical Sciences, University of Naples Federico II, Via Cintia 4, 80126 Napoli, Italy*
[b] *Departament de Bioquímica i Biologia Molecular, Institut de Biotecnologia i Biomedicina, Universitat Autònoma de Barcelona, 08193 Bellaterra, Barcelona, Spain*
[c] *Department of Chemistry, Graduate School of Science, Osaka University, 1-1 Machikaneyama, Toyonaka, Osaka 560-0043, Japan*
[d] *Instituto de Biología Molecular de Barcelona (IBMB-CSIC), Parc Científic de Barcelona, Baldiri Reixac 10, 08028 Barcelona, Spain*
[e] *Laboratori de Recerca en Microbiologia i Malalties Infeccioses, Hospital Universitari Parc Taulí, Institut d'Investigació i Innovació Parc Taulí (I3PT-CERCA), UniversitatAutònoma de Barcelona, Sabadell, Spain*
[f] *Institute for Research in Biomedicine (IRB Barcelona), Barcelona Institute of Science and Technology, 08028 Barcelona, Spain*
[g] *Department of Pharmacy, University of Naples Federico II, Via Domenico Montesano 49 - 80131 Napoli Italy*

ARTICLE INFO

Keywords:
Bacterial lectins
Sialoglycans
Molecular recognition
STD NMR

ABSTRACT

Mycoplasma pneumoniae and *Mycoplasma genitalium* are two emerging bacterial pathogens that colonize the human respiratory and urogenital epithelia, respectively. Both pathogens express cell surface cytoadhesins that play a crucial role in the interaction with the host, mediating the attachment to sialylated glycan receptors and triggering infection. The design of competitive binding inhibitors of *Mycoplasma* cytoadhesins has potential to disrupt these interactions and lessen bacterial pathogenesis. To this end, we report here molecular insights into the adhesion mechanisms of *M. pneumoniae* and *M. genitalium*, which are largely mediated by sialylated glycans on the host cell surface. In detail, a combination of Nuclear Magnetic Resonance (NMR) spectroscopy, fluorescence analysis and computational studies allowed us to explore the recognition by the cytoadhesins P40/P90 in *M. pneumoniae* and P110 in *M. genitalium* of sialylated *N*- and *O*-glycans. We reveal that, unlike other bacterial adhesins, which are characterized by a wide binding pocket, *Mycoplasma* cytoadhesins principally accommodate the sialic acid residue, in a similar manner to mammalian Siglecs. These findings represent crucial insight into the future development of novel compounds to counteract *Mycoplasma* infections by inhibiting bacterial adherence to host tissues.

1. Introduction

Bacterial adhesion to host cells is one of the initial stages of infection and is a key step in pathogenesis. This process is mediated by dedicated bacterial surface structures that enable microorganisms to specifically target host molecular signatures such as carbohydrate signalling molecules [1]. Several *Mycoplasma* species, including *Mycoplasma pneumoniae* and *Mycoplasma genitalium*, have been shown to infect host cells via this adhesion pathway [2,3]. Mycoplasmas are cell wall-less microorganisms, phylogenetically related to Gram-positive bacteria, and are

Abbreviations: CAPs, Community-Acquired Pneumonias; PID, Pelvic Infiammatory Disease; 3'SLn, 3' Sialyl *N*-acetyl lactosamine; 6'SLn, 6' Sialyl *N*-acetyl lactosamine; sTa-Thr, Sialyl-T-antigen; Neu5Ac, *N*-acetyl Neuraminic acid; Gal, galactose; GalNAc, *N*-acetyl galactosamine; Glc*N*Ac, *N*-acetyl glucosamine; SPR, surface plasmon resonance; NHAc, acetamide; NMR, Nuclear Magnetic Resonance; STD NMR, Saturation Transfer Difference NMR; COSY, Correlation Spectroscopy; TOCSY, Total Correlation Spectroscopy; NOESY, Nuclear Overhauser Effect Spectroscopy; HSQC, Heteronuclear Single-Quantum Coherence; SLBR, Siglec-like Binding Region; tr-NOESY, transferred-NOESY; MM, Molecular Mechanics; MD, Molecular Dynamics; NOE, Nuclear Overhauser Effect; Siglecs, Sialic Acid-Binding Immunoglubuline-Type Lectins; SNFG, Symbol Nomenclature For Glycans; PCR, Polymerase Chain Reaction.

* Corresponding author.
E-mail address: roberta.marchetti@unina.it (R. Marchetti).
[1] Equal contribution.

https://doi.org/10.1016/j.ijbiomac.2024.135277
Received 29 February 2024; Received in revised form 26 July 2024; Accepted 31 August 2024
Available online 1 September 2024

capable of invading and replicating within eukaryotic cells [4]. Among these species, *M. pneumoniae* is an exclusively human parasite that [5] primarily affects the conducting airways, and is the leading cause of upper and lower respiratory tract infections [6,7].It is estimated that *M. pneumoniae* is responsible for up to 40 % of community-acquired pneumonias (CAPs) in children and adults worldwide. Atypical CAPs, also caused by *M. pneumoniae*, may also involve extrapulmonary organs, including, for example, head, eyes, ears, skin, or gastrointestinal tract [8]. On the other hand, *M. genitalium* is a sexually transmitted bacterium that frequently co-infects the urogenital tract with other pathogens, such as HIV, *C. trachomatis*, and *N. gonorrhoeae* [9]. In women, it is responsible for several inflammatory reproductive tract syndromes, including cervicitis, pelvic inflammatory disease (PID), and infertility [10]; in men, it is the leading cause of 30–40 % cases of urethritis [11]. Additionally, *M. genitalium* has been associated with preterm birth, spontaneous abortion, and HIV acquisition [12].

Cytoadherence and gliding motility of these two pathogens are essential for colonization of the human tissues and are mediated primarily by a complex attachment organelle that consists of an intracellular region and a specialized surface-exposed structure. This surface structure comprises accessory proteins [13] that form the adhesion complex, a peplomer-like structure termed Nap [14]. The Nap is essential for infectivity and displays a tetrameric organization composed of heterodimers of the cytoadhesin proteins P140 and P110 in *M. genitalium*, and their homologs P1 and P40/P90 in *M. pneumoniae* [15,16].These cytoadhesins possess a similar domain organization, consisting of a large extracellular domain (the crown), a transmembrane helix, and a short cytoplasmic tail (C-domain). The extracellular portion is further divided into two subdomains: a small *C*-terminal domain and an *N*-terminal region containing a seven-bladed β-propeller in the shape of a crown, where the sialic acid binding site is located [17]. Given the similar topology of the cytoadhesin structures of *M. genitalium* and *M. pneumoniae* and neuraminidase proteins from influenza A viruses, it has been suggested that P110 and P40/P90 proteins contain a putative catalytic site, located close to the sialic acid binding site [18] and characterized by the presence of an RLP (Arg-Leu-Pro) motif (see Fig. S2) usually found in non-viral sialidases [19,20].

Sialic acids are negatively charged nine-carbon monosaccharides, found in abundance on cell surface structures of humans and other mammals and involved in various biological functions, including cell adhesion and immune responses. This class of monosaccharides, often at the terminal end of both *N*- and *O*-glycans on cell surfaces, can act as receptor ligands for certain pathogens, allowing them to attach and infect host cells [21]. The interaction of *Mycoplasma* adhesins with specific sialylated glycans on target host cells has been shown to be a prerequisite for the development of Mycoplasmas-associated infectious diseases [22,23].

.Given the critical roles that *Mycoplasma* cytoadhesins play in bacterial adhesion to host cells, they are attracting increasing attention as promising targets for anti-adhesive therapy of *Mycoplasma* infections. Notably, anti-adhesive agents are not bactericidal and therefore much less likely than antibiotics to induce the evolution and spread of resistant strains.

We previously elucidated the structural features of the main cytoadhesins from *M. genitalium* and *M. pneumoniae* [18], and cryo-electron tomography studies have been recently published describing the structure of the major adhesion complex from *Mycoplasma genitalium* [24] however, the resolution of the cryo-ET data was not sufficient to visualize the sialylated oligosaccharides and the adhesion mechanism of *Mycoplasma* cells remains not fully understood. Thus, further molecular insights on sialoglycan recognition and binding by *Mycoplasma* cytoadhesins are needed to design effective anti-adhesion strategies, either by reducing the contact between host tissues and pathogens, and/or by prevention of adhesion of the infectious agent. To further this aim, we dissect herein the recognition profiles and binding modes of P110 from *M. genitalium* and P40/P90 from *M. pneumoniae* with sialoglycans typically decorating the host cell surfaces [25]. We employ an integrated approach that combines NMR spectroscopy, fluorescence analysis, and computational studies, rendering in three-dimensional, atomic-level detail, the adhesin-sialoglycan complexes. These findings accurately defined the ligand-epitope maps and their bioactive conformations, together with the protein structural features involved in sialoglycan recognition and their respective binding affinities. In addition, our outcomes allow us to pinpoint molecular differences in the sugar-binding mode of *Mycoplasma* cytoadhesins with respect to other bacterial Siglec-like adhesins, such as those expressed by streptococcal species [26].

Given the high incidence of pathologies related to *M. pneumoniae* and *M. genitalium*, the absence of a vaccine for *M. pneumoniae* in contrast to other respiratory pathogens, and the rapid increase of antibiotic resistance of Mycoplasma pathogens [27], our results are of critical importance and lay the foundation for the future development of therapeutic strategies based on the inhibition of *Mycoplasma*-host cell adhesion and infection Mycoplasma.

2. Results

The association between *Mycoplasma* cytoadhesins (P110 from *M. genitalium* and P40/P90 from *M. pneumoniae*) and common *N*- and *O*-glycans (Fig. S1) abundant on the host mucosal surfaces, both in human respiratory and reproductive tract, was initially assessed by fluorescence spectroscopy (Figs. 1 and S3). Briefly, a fixed concentration of both proteins was titrated with increasing amounts of each sialoglycan (3'SLn, 6'SLn, biantennary *N*-glycans, sTa and sTa-Thr) to derive the binding isothermal curves for all protein-ligand mixtures and, consequently, obtain information regarding the binding affinities. The results demonstrated the ability of both cytoadhesins (P110 and P40/P90) to similarly recognize different Neu5Ac (*N*-acetyl Neuraminic acid)-containing ligands, as the estimated binding constants (K_b) were all in the micromolar range (Figs. 1 and S3). Notably, these findings align with equilibrium dissociation constants previously established through surface plasmon resonance (SPR) measurements [15,16].

To elucidate the mechanism of cell adhesion and gliding of *M. genitalium* and *M. pneumoniae*, the molecular recognition of the different sialylated ligands by cytoadhesins was further investigated by using complementary techniques. As described in the following sections, Saturation Transfer Difference NMR (STD NMR) was applied to reveal the ligand binding epitopes and transferred-NOESY (tr-NOESY) experiments were employed to investigate their conformational behavior [28]. In combination with NMR results, Molecular Dynamic (MD) simulations were also carried out to provide 3D models of the complexes.

2.1. 3'SLn recognition by P110 and P40/P90

The analysis of the STD NMR spectra of the mixture P110/3'SLn clearly showed that the protein binding pocket was selective toward the Neu5Ac moiety (Fig. 2A, left panel). As suggested by the STD NMR enhancements, the entire Neu5Ac was recognized by the receptor and received a good magnetization transfer from P110. The strongest relative STD NMR effect belonged to the acetyl group of Neu5Ac unit, followed by the protons H6 and H7, which had an STD NMR percentage above 40 %. Other protons of Neu5Ac (H4, H5, H8 and H9) showed STD signals but to a lesser extent. The other sugar residues did not participate in the recognition process, in agreement with the crystal structure of P110 in complex with 3'SLn [15].

Tr-NOESY experiments and MD simulations then allowed us to describe the ligand's bioactive conformation. The conformational behavior of 3'SLn has been extensively analyzed in free solution and displays an equilibrium between different conformations, namely t, *g* and -*g*, according to the different values of the Φ(C1-C2-O-C3') dihedral angle around the Neu5Ac-α-(2,3)- Gal (galactose) glycosidic linkage [29]. Here, the conformation of the ligand in the presence of P110 was

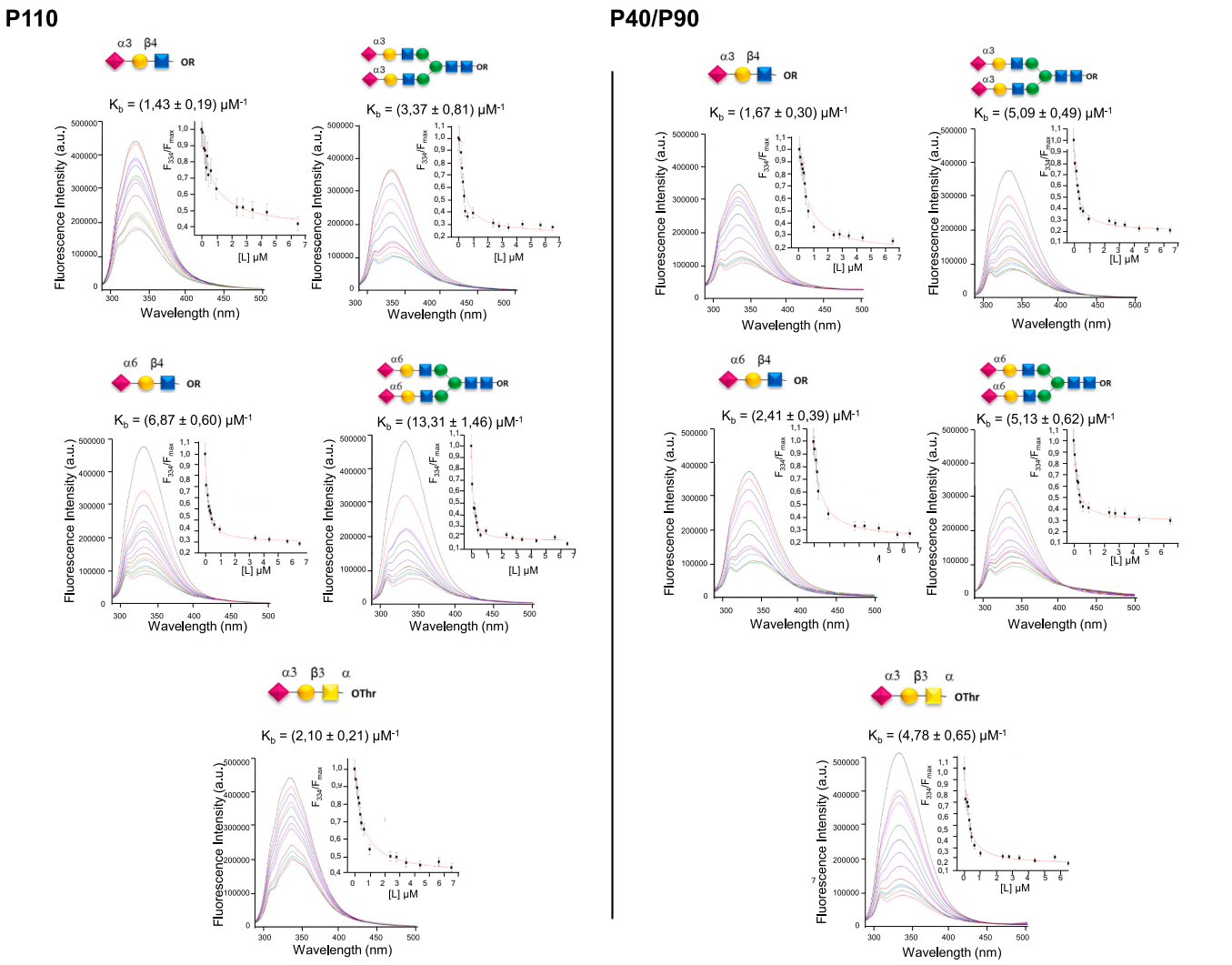

Fig. 1. Measurement of sialoglycans affinity for P110 and p40/P90 by fluorescence spectroscopy. Quenching of intrinsic fluorescence of *M. genitalium* P110 (left panel) and *M. pneumoniae* P40/P90 (right panel) in the presence of increasing amounts of 3'SLn, 6'SLn, sTa-Thr and biantennary sialoglycans, respectively. The binding isotherms were obtained by plotting the values of F/F_{max} versus the total ligand concentration, where F is the fluorescence intensity observed at each addition of ligand, and F_{max} is the maximum fluorescence intensity observed. The resulting binding constants (K_b) were reported in the insets. Error bars indicate standard deviations of representative experiments performed in triplicate.

analyzed; the glycosidic torsion trajectories of 3'SLn were monitored during a simulation of the bound state within the P110 binding pocket and indicated a preference of the ligand for the t conformer (Fig. S4). This agreed with the tr-NOESY derived calculated distances for 3'SLn in the presence of P110 (Fig. 2A, right panel). In particular, the presence of the key NOEs between the diastereotopic protons at position 3 of the Neu5Ac and the proton H3 of the Gal residue, as well as the absence of the H3 Gal – H8 Neu5Ac NOE contact, suggested that the 3'SLn mainly adopted a t conformation in solution when accommodated in the protein binding pocket.

A cluster analysis of the MD (Fig. 3) indicated that the sialic acid was the main residue involved in the binding interaction between P110 and 3'SLn, in agreement with the STD NMR results. In addition, numerous hydrogen bonds were predicted at the protein-ligand interface; for example, H-bonds were established between Neu5Ac carboxyl group and Arg600 and Ser458. Asn200 exhibited two interactions with Neu5Ac, one with the OH at position 4 and the other with its acetamide moiety, while Pro197 formed a H-bond with the hydroxyl proton 7 of Neu5Ac. In addition, Asn475 established crucial H-bonds with hydroxyl protons 8 and 9 of the glycerol chain of Neu5Ac, which strongly contributed to the stabilization of the complex and resulted in the flexible loop region (471–482 aa) moving closer to the Neu5Ac binding site (Fig. 3A, see also Fig. S4 left panel). As shown in Fig. 3A, the ligand was positioned with the acetamide group of the Neu5Ac in a hydrophobic pocket close to Phe457, which also helped to stabilize the binding. Another significant contact was observed between the amide nitrogen of Neu5Ac and Ser456, forming a hydrogen bond that was stable during the MD simulation, in accordance with the high STD contribution.

Upon comparison of these results to the interactions observed in the crystal structure of P110 in complex with 3'SLn [15], it was evident that most of contacts align with previous findings, mainly involving the residues Ser458, Ser456, Asn200 and Pro197, although in the crystal the ligand is accommodated in the protein binding site with a different conformation relative to that derived from the NMR data (Fig. 4A).

Analogously, the recognition of 3'SLn by the *M. pneumoniae* cytoadhesin P40/P90 was studied. Similarly to P110, the STD NMR analysis revealed a selective binding mode mainly involving the Neu5Ac moiety (Fig. 2B, left panel). The highest magnetization transfer was again observed for the acetyl group of Neu5Ac. The proton at position 7 of the Neu5Ac also exhibited a significant STD effect above 50 %, while the protons H5, H6, and H9 contributed to the binding but with lower

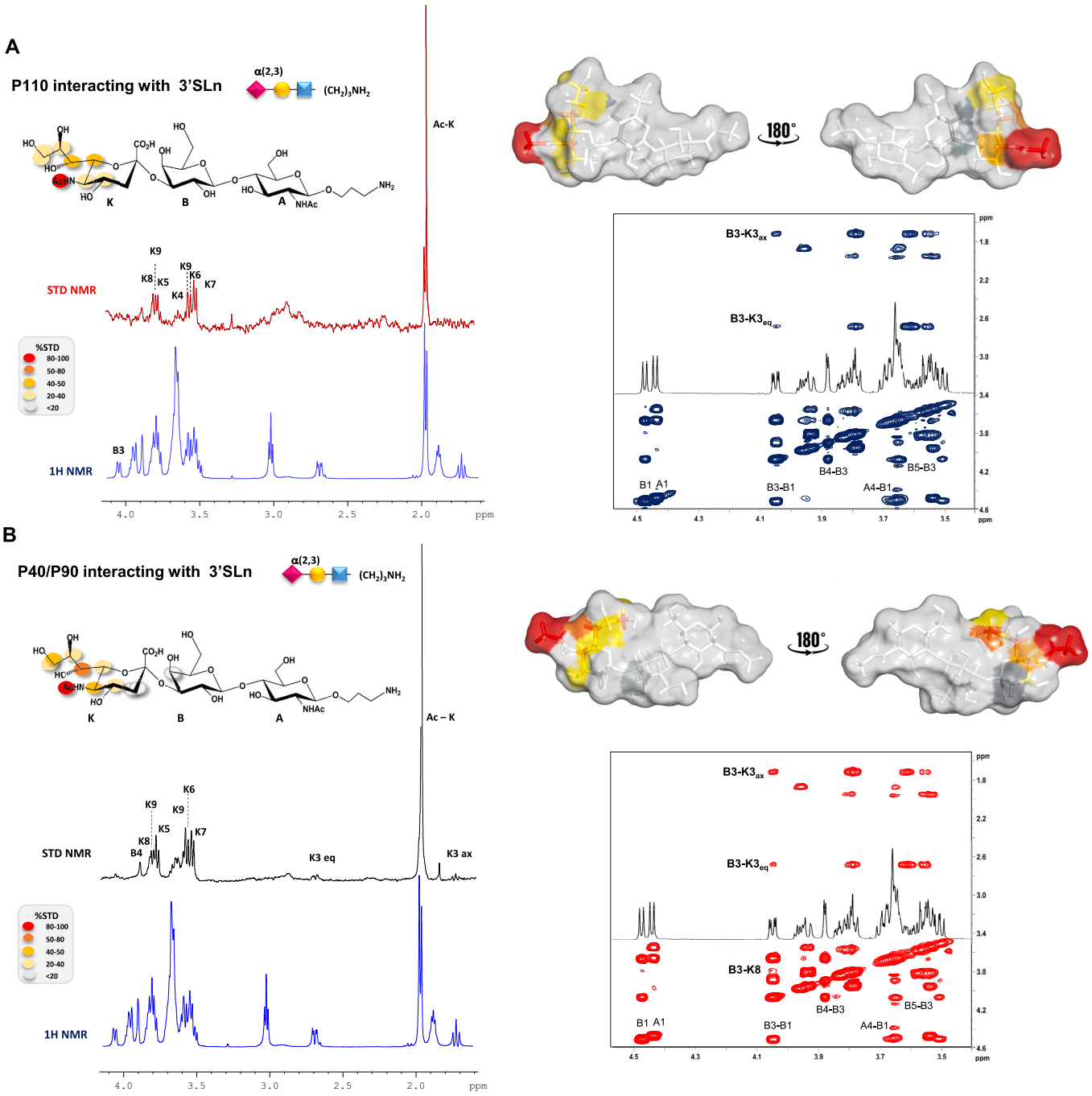

Fig. 2. NMR analysis of 3'SLn bound to P110 and P40/P90. A) Superimposition of the STD NMR spectrum (red) and the unsaturated reference spectrum (blue) of 3'SLn interacting with P110.The ligand epitope map has been calculated by $(I_0 - I_{sat})/I_0$, where $(I_0 - I_{sat})$ was the signal intensity in the STD-NMR spectrum and I_0 was the peak intensity of the off-resonance spectrum Tr-NOESY spectrum on the 1:50 P110–3'SLn mixture and the ligand bioactive conformation are showed on the right. The ligand surface was colored according to the STD-derived epitope mapping. B) The superimposition of STD NMR spectrum (black) and the unsaturated reference spectrum (blue) together with the epitope map of the 3'SLn interacting with P40/P90 are reported on the left. Tr-NOESY spectrum of 1:50 P40/P90–3'SLn mixture and STD-derived epitope mapping of 3'SLn in its bioactive conformation are showed on the right.

STD percentages between 50 % and 20 %. Very slight STD enhancements were also observed for the diastereotopic protons of the Neu5Ac and the proton at position 4 of the Gal unit.

Computational studies were also performed to further describe the conformational behavior of 3'SLn upon binding to P40/P90. In accordance with tr-NOESY data (Fig. 2B, right panel), MD results revealed that 3'SLn could be accommodated in the binding pocket upon adopting two different conformations, namely *t* and *-g*, with the Φ dihedral angle around the glycosidic linkage between Neu5Ac-Gal at 180° and − 60°, respectively. This is likely due to the higher flexibility (see Fig. S4, right panel) and the different orientation of a loop region (642–653 aa) of P40/90 relative to P110, resulting in a wider binding pocket.

Regardless of the conformation adopted by the ligand, the main interactions with the protein were established only with the Neu5Ac moiety, as already revealed by the NMR analysis and in agreement with the previously published X-ray data (Fig. 4B). Indeed, in the main representative conformation of the complex (Fig. 3B), the Neu5Ac was the only sugar residue entirely accommodated in the protein binding pocket, while Gal and Glc*N*Ac residues were more distant from the protein surface. Specifically, a stable contact occurred between the

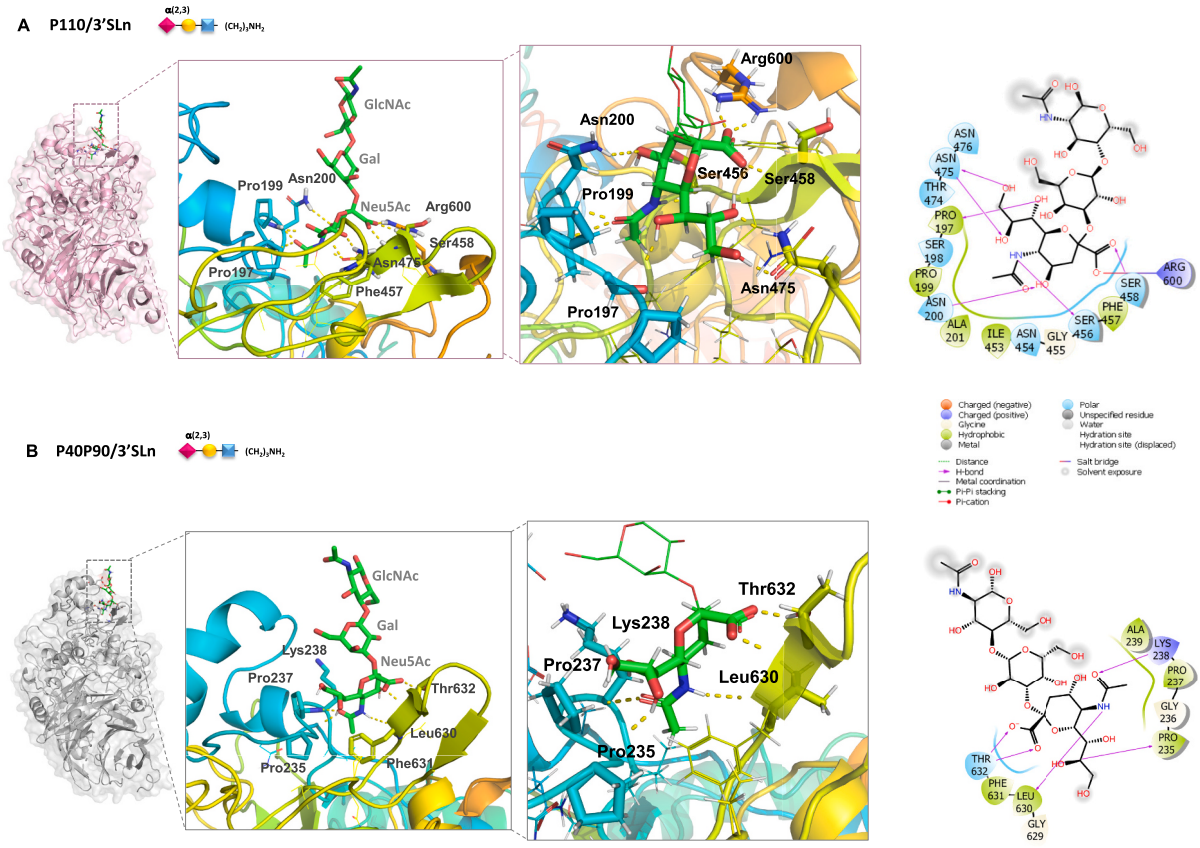

Fig. 3. P110–3'SLn and P40/P90–3'SLn predicted complexes. A) 3D view of P110–3'sLn predicted complex. B) 3D view of P40/P90–3'sLn complex. The aa of the binding pocket involved in the binding with Neu5Ac are represented as sticks. The flexible loop moving closer to the binding site upon binding is represented in yellow. For clarity, a zoom on the Neu5Ac is also reported. On the right, two-dimensional plots highlighting the main protein-ligand interactions are shown. Solid arrows represent hydrogen bonds with the functional groups of the backbone; the other residues in the binding pocket participate in polar and hydrophobic interactions.

amide group at position 5 of Neu5Ac and the Leu630 that was present for about 70 % of MD simulation time.

The Neu5Ac carboxyl group also established H-bonds with the side chain of Thr632. Consistent with STD NMR results, the OH at position 7 interacted with Pro235 and the oxygen of the acetyl moiety established a contact with Lys238. The presence of hydrophobic residues near the binding site, in particular Phe631, contributed to stabilize the complex and anchor the Neu5Ac unit to the protein via hydrophobic contacts.

2.2. 6'SLn recognition by P110 and P40/P90

The binding mode and the conformational behavior of 6'SLn when interacting with P110 and P40/P90 were also investigated by combining NMR experiments and computational approaches. Also in this case, in accordance with the previous crystallographic data (Fig. 4 lower panel), Neu5Ac was the ligand motif most involved in cytoadhesin binding. The STD NMR analysis and the resulting epitope map of 6'SLn bound to P110 showed that the highest STD NMR effect was given by the acetyl group of Neu5Ac (Fig. S5). Also, the proton H7 contributed significantly to the interaction, with a STD NMR relative percentage close to 50 %. A minor contribution was given by H6, H8 and H9 protons of the Neu5Ac.

MD data corroborated the experimental results, clearly indicating the key role of the sialic acid in the binding interaction and showed numerous H-bonds established between the protein amino acids and the terminal Neu5Ac residue, also stabilized by hydrophobic contacts with Phe457 (Figs. 5 and S6). Recurring interactions above 90 % of the simulation time were formed between Pro197 and the Neu5Ac hydroxyl group at position 7, while the amide group established an interaction with the carbonyl oxygen of Ser456. Other H-bonds occurred between Asn200 and both the carbonyl oxygen of the acetyl moiety and the OH at position 4. The hydroxyl protons at positions 8 and 9 of the glycerol chain of Neu5Ac interacted with Asn475. In addition, the hydroxyl group of Ser458 also mediated a crucial interaction with the carboxyl group of Neu5Ac. While the Neu5Ac was the residue most involved in the interaction, in all the complexes derived from the MD cluster analysis, transient interactions between the protein and some protons of the GlcNAc unit were also predicted.

Consistent with the results observed for the cytoadhesin P110, the STD-NMR experiments acquired on the mixture P40/P90–6'SLn suggested that the protein selectively recognized the Neu5Ac residue (Fig. 5). As shown by the epitope map (Fig. S5), the most involved group was the acetyl moiety of the Neu5Ac; protons H6 and H7 also exhibited high STD enhancements upon 50 %, while the glycerol chain and the other protons of Neu5Ac contributed less to the interaction. These data agreed with MD results and the previously published crystallographic complex showing that 6'SLn established a crucial interaction with amino acids of the binding pocket mainly via the Neu5Ac residue. In detail, its carboxyl group formed a H-bond with Thr632 [17]; the acetamide group of Neu5Ac interacted with the Leu630 and Lys238; and the Pro235 displayed an interaction with the hydroxyl group at position 8 of the glycerol side chain.

As already predicted for the complexes with 3'SLn, MD simulation analysis also revealed higher flexibility of the ligand when bound to P40/P90 than with P110. Given the presence of the additional ω torsion angle in the 6'SLn with respect to 3'SLn, the ligand could sample a population distribution in equilibrium between different rotamers,

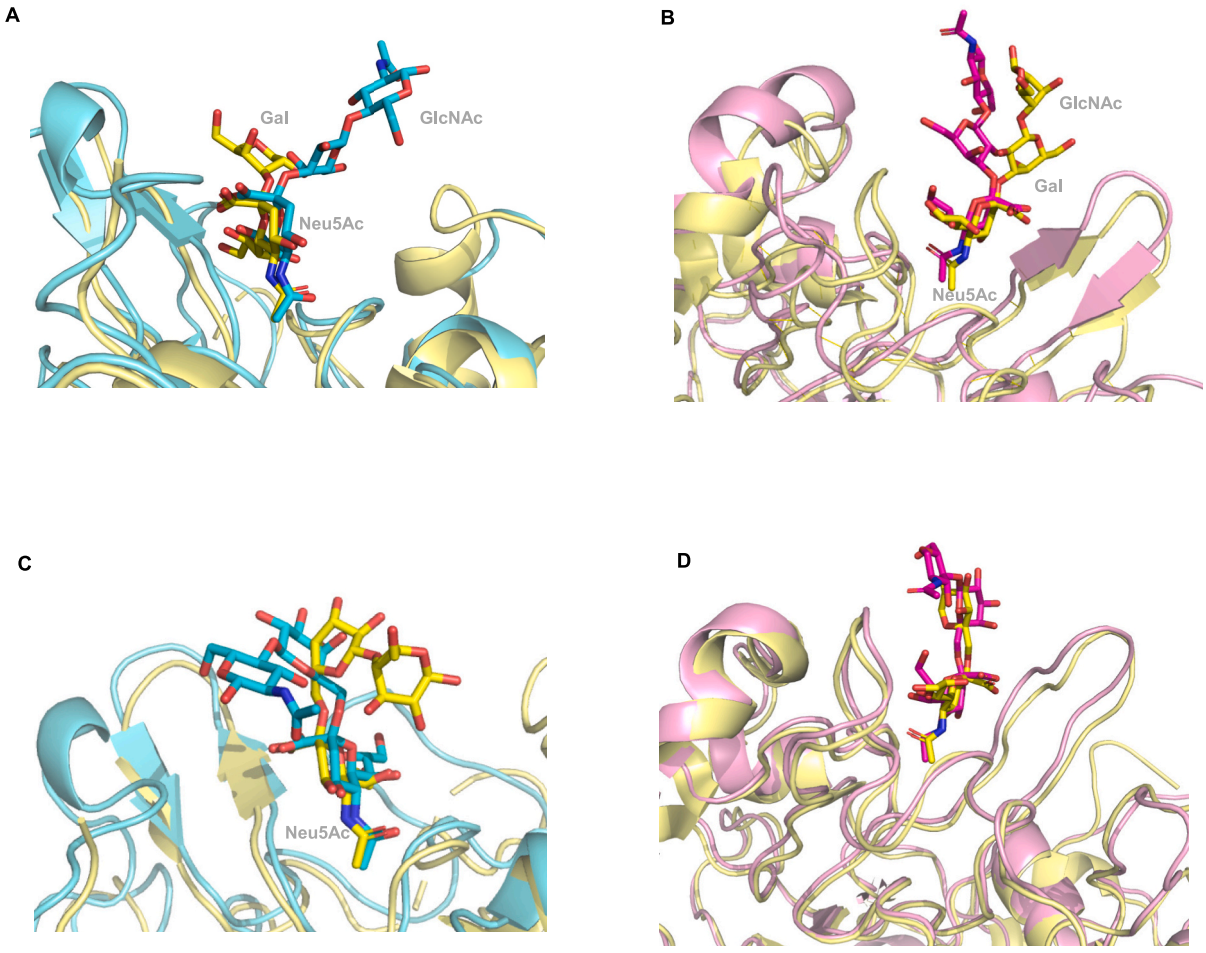

Fig. 4. Superimposition of P110 and P40/P90 - sialoglycans complexes derived from MD simulations and X-Ray. Upper panel: Superimposition of P110–3'sLn and P40/P90–3'sLn complexes. A) 3D view of the P110–3'sLn complexes as derived by MD simulation (in cyan) and from crystallographic analysis (PDB: 6r41 in yellow). B) 3D view of the P40/P90–3'sLn complexes as derived by MD simulation (in pink) and from crystallographic analysis (PDB: 6tlz in yellow). Lower panel: Superimposition of P110–6'sLn and P40/P90–6'sLn complexes. C) 3D view of the P110–6'sLn complexes as derived by MD simulation (in cyan) and from crystallographic analysis (PDB: 6r43 in yellow). D) 3D view of the P40/P90–6'sLn complexes as derived by MD simulation (in pink) and from crystallographic analysis (PDB: 6tm0 in yellow).

namely *gt*, *tg* and *gg*, according to the different values of ω angle (60°, 180° and − 60° respectively) [30].Specifically, in the free state, the *gt* and *tg* rotamers were the most populated, while the *gg* rotamer population was minor. Interestingly, MD results revealed that, upon binding to P110, the ligand was mainly accommodated in the *gt* conformation (Fig. S6). On the other hand, when 6'SLn bound to P40/P90, an equilibrium was observed between two different rotamers (*gt* and *tg*) that were similarly accommodated in the protein binding pocket, with the *tg* conformation as the more populated one.

2.3. Recognition of complex type N-glycans by P110 and P40/P90

To acquire additional insights into *N*-glycans recognition by P110 and P40/P90, longer ligands, which mimic natural complex type biantennary *N*-glycans containing the Neu5Ac-α-(2,3)-Gal or Neu5Ac-α-(2,6)–Gal epitopes at their terminal end, were also investigated (see supporting information). STD-NMR analyses carried out on branched undecasaccharides (Figs. 6 and S7) reinforced selective protein recognition for the Neu5Ac residues, whereas the other sugar units did not contribute to the binding process. These results were comparable with those obtained on smaller trisaccharides. Again, the acetyl group of the Neu5Ac displayed the highest STD enhancement, while some other STD signals of strong intensity belonging to the protons of the sialic acid sugar backbone, in particular H7 and H6, were also observed. On the contrary, the resonances of the protons belonging to the other sugar units were not visible in the spectra, indicating that they were solvent exposed. These data were in full agreement with the results of MD simulations. Indeed, as showed in the predicted model depicted in Fig. 6, the longer, complex N-glycan was anchored to the protein surface with the sialic acid on one antenna mainly establishing polar contacts with Leu634 and Thr632 and hydrophobic interactions involving Phe631, as previously reported for the trisaccharide ligand. Moreover, additional interactions were predicted in the model between the Neu5Ac unit positioned at the terminal end of the other glycan branch and Arg226 and Ser227 residues. This result agreed with the values of the binding constants measured by fluorescence analysis, which revealed a protein affinity for each undecasaccharide that was approximately two-fold higher than the one measured for the corresponding trisaccharide, further supporting the possibility of a branched binding mode involving both sialic acid residues on the longer sialoglycans.

2.4. sTa-Thr recognition by P110 and P40/P90

The molecular basis of the interactions between *Mycoplasma*

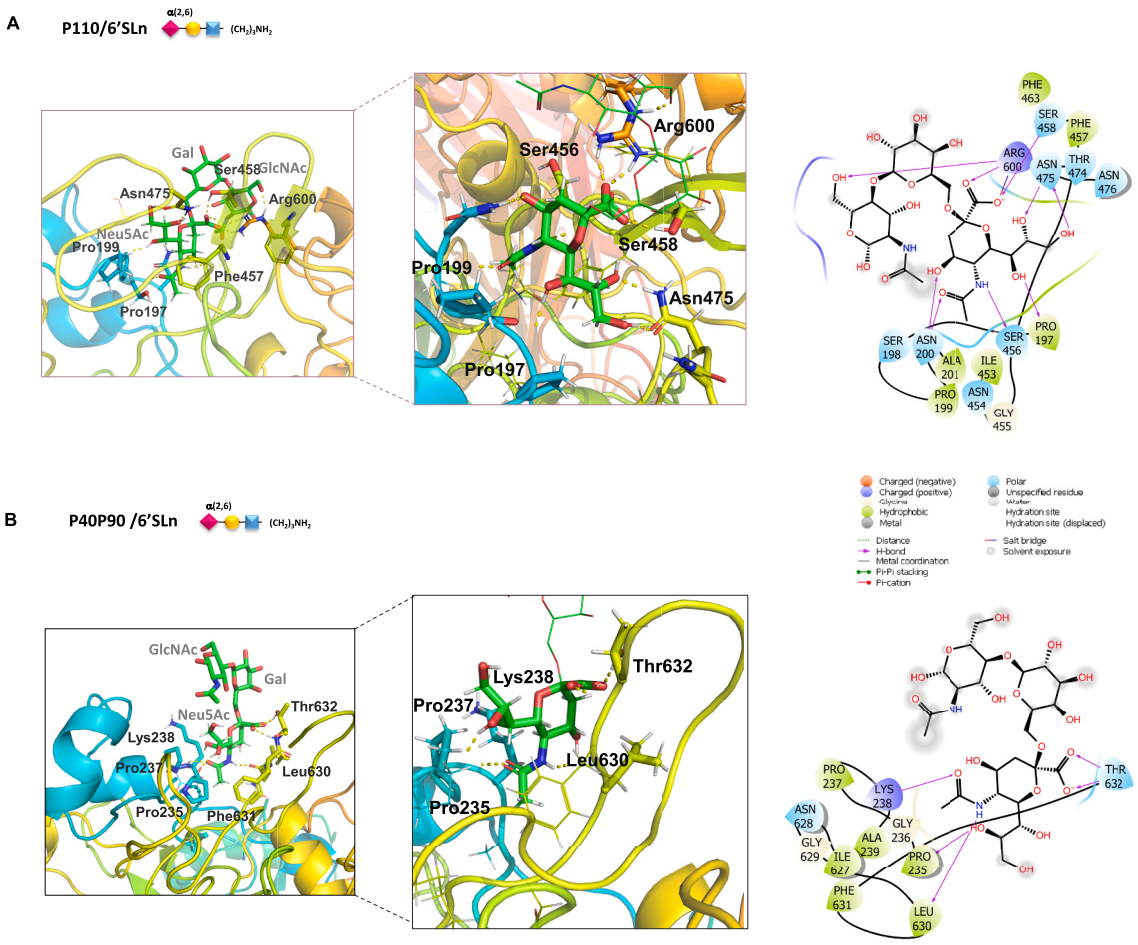

Fig. 5. P110–6'SLn and P40/P90–6'SLn predicted complexes. A) 3D view of the P110–6'sLn complex. B) 3D view of the P40/P90–6'sLn complex. The aa of the binding pocket involved in the binding with Neu5Ac are represented as sticks. Two-dimensional plots highlighting the main protein-ligand interactions are also reported. Solid arrows represent hydrogen bonds with the functional groups of the backbone; the other residues in the binding pocket participate in polar and hydrophobic interactions.

cytoadhesins and the ad hoc synthesized, threonine-linked sialyl-T-antigen, sTa-Thr, was also assessed. As revealed by the STD NMR analysis, both proteins were able to recognize the *O*-glycan in a similar manner (Fig. 7). The STD NMR spectra showed that the Neu5Ac displayed the highest STD contribution, the galactose unit slightly contributed to the interaction, and the reducing Gal*N*Ac (*N*-acetyl galactosamine), as well as the Thr residue, did not receive any magnetization transfer from the protein.

Regarding P110, the acetyl group of Neu5Ac showed a strong contribution to the binding, followed by H7, H5, H6, H8 and H9 protons, which displayed STD NMR relative percentages upon 50 %. On the other hand, H4 of Neu5Ac and H4 and H6 of the Gal were less involved in the binding event, showing %STD values below 40 %.

In the case of P40/P90, a strong saturation transfer was also detected for the acetyl group and H7 of the Neu5Ac, showing the highest STD NMR effects (Fig. 7). H4, H5 and H9 further contributed to the binding with STD NMR enhancements greater than 50 %. Protons at positions 8, 6 and 3 of the Neu5Ac chain underwent less magnetization transfer exhibiting a %STD NMR lower than 50 %. Moreover, slight STD effects were observed also for the galactose moiety that exhibited a weaker contribution to the binding; galactose protons H4, H3, H6 and H2 displayed STD NMR percentages lower than 20 %.

Once the ligands interacting epitopes were established, the binding profile of the complexes of P110 and P40/P90 with sTa-Thr were further investigated via computational approaches and tr-NOESY analysis. As shown in Fig. 8, the sTa-Thr was accommodated in the same protein binding pocket as the previously analyzed ligands. Regarding the P110/sTa-Thr predicted complex, interactions occurred between Pro197 and the hydroxyl group at position 7 of Neu5Ac and between Ser456 and the amide nitrogen of the sialic acid. The Asn200 residue also interacted with the OH group at position 4 of Neu5Ac and Ser458 established two H-bonds with the carboxyl group of this residue, as seen in the crystal structures [15,17].Also, the MD simulation of P40/P90 in complex with sTa-Thr revealed a selective recognition toward Neu5Ac. The most stable contact occurred between Leu630 and the amide group of Neu5Ac, according to the observed high STD NMR value. The Neu5Ac carboxyl moiety also established stable H-bonds with Thr632. Other significant contacts were predicted for OH at C7 of Neu5Ac, forming a hydrogen bond with Pro235, which was stable during the MD simulation in accordance with the high STD contribution of H7 (around 80 %). In addition, Lys218 formed a hydrogen bond with the Neu5Ac acetyl group.

The trajectories of ligand glycosidic torsions were sampled during the MD simulations in the free and bound states for both systems to evaluate the sTa-Thr conformational behavior (Fig. S8). The sTa-Thr shape and conformation were mainly influenced by the glycosidic torsion angles, namely ϕ (C1-C2-O-C3')/ψ (C2-O-C3'-H3') around Neu5Ac-α-(2,3)-Gal and ϕ (H1–C1–O–C3')/ ψ (C1–O–C3'–H3') around the Gal-β-(1,3)–GalNAc bonds. Interestingly, a conformer selection was observed upon binding with P110. Indeed, in the bound state only the minimum characterized by the value of ϕ torsional angle at −60° was populated. On the other hand, no significant conformational differences

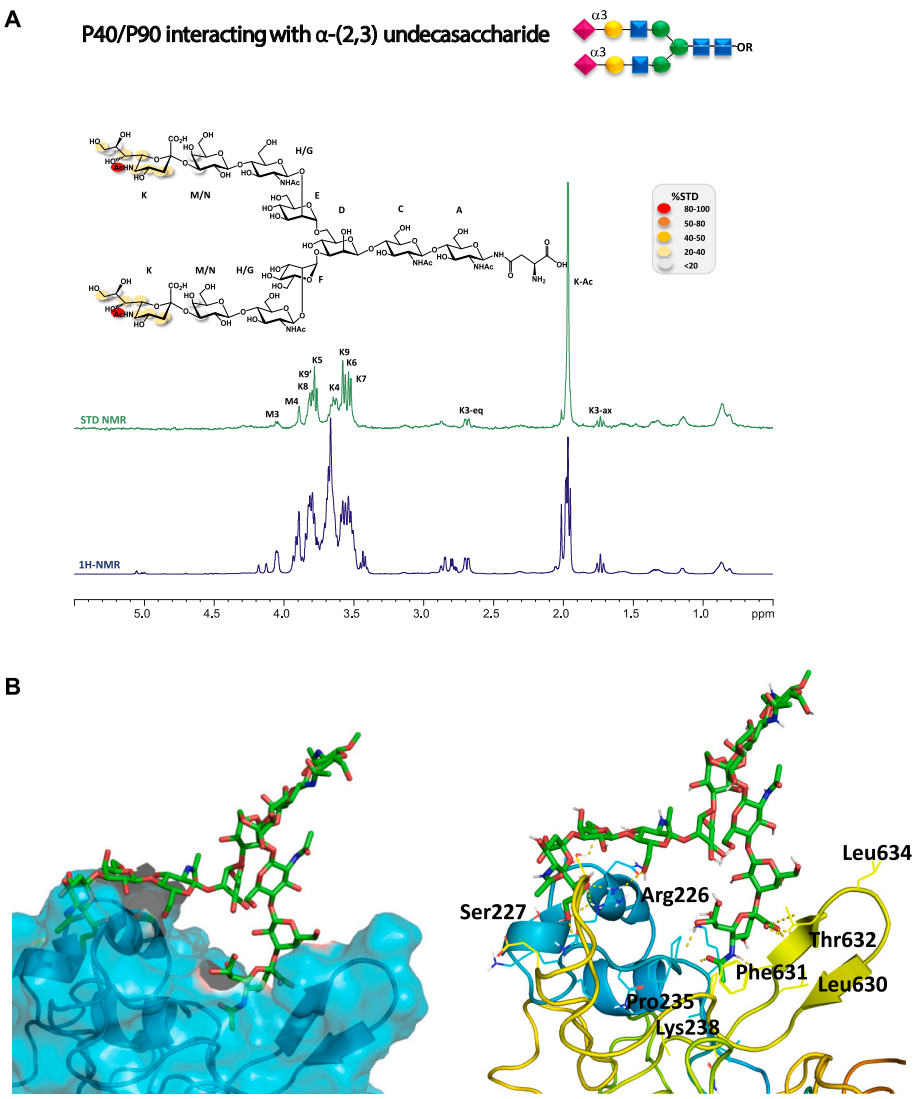

Fig. 6. NMR and MD analysis of complex glycan bound to P40/P90. A) STD-NMR spectrum (green) and the unsaturated reference spectrum (blue) of the undecasaccharide containing the Neu5Ac-α-(2,3)-Gal epitope at its terminal end interacting with P40/P90. The ligand epitope map is also showed. B) 3D view of the P40/P90-undecasaccharide predicted complex.

between the free and bound state were observed for the sTa-Thr interacting with P40/P90, which mainly adopted two conformations with the ϕ torsion angle along the Neu5Ac -α-(2,3)-Gal unit at 180° and − 60°.

3. Discussion

Sialic acid-containing glycans are highly abundant on vertebrate cell surfaces and play essential roles in a plethora of biological functions of relevance both in healthy and diseased states. They serve as critical modulators of cell division, cell signalling, and cell-cell recognition, regulating a wide range of immune responses. Thus, it is not surprising that many pathogenic organisms, including bacteria and viruses, have evolved to exploit host sialoglycans to facilitate the first steps of their infections. As example, it has been extensively reported that α-2,3- and α-2,6- sialoglycans, widely exposed on the human respiratory tract, allow bacterial and/or viral association with and entry into target cells [31].Moreover, several bacterial species, including *Mycoplasma* genus, have been shown to interact with sialylated glycoproteins on the exterior of eukaryotic cells to mediate adhesion and subsequent infection [32–34]. In particular, sialylated glycoproteins, such as laminin, exhibiting terminal α-2,3-linked sialic acids, have been showed to support *M. pneumoniae* adherence and gliding motility [3,22]. Additionally, it has been previously demonstrated that heavily sialylated mucins are implicated in the attachment of *M. genitalium* to human vaginal/cervical mucosa [35].

Given the increasing emergence of antibiotic resistance documented in Mycoplasmas, such as the respiratory and urogenital pathogens *M. pneumoniae* and *M. genitalium* respectively, the development of alternative therapeutic strategies to prevent and combat Mycoplasmas-associated infections is urgently needed. Specifically, interference with this sialylated glycoprotein-mediated adhesion pathway represents a promising therapeutic route to treat *Mycoplasma* infection.

Despite recent efforts to understand the mechanism of this bacterial adhesion pathway, the molecular basis of the interaction remained obscure. We report here the atomic-level characterization of the recognition modes of the *Mycoplasma* cytoadhesins, P40/P90 and P110, interacting with host sialylated *N*- and *O*-glycans.

To elucidate in-depth the structural details of sialoglycans recognition by bacterial cytoadhesins, a combination of biophysical techniques and computational methods were employed. This integrated approach allowed us to compare the P110 and P40/P90 binding mode, to identify the ligand epitopes accommodated in the protein binding site, to explore the conformational behavior of *N*- and *O*-glycans interacting with the bacterial cytoadhesins, and to predict 3D models of protein-ligand

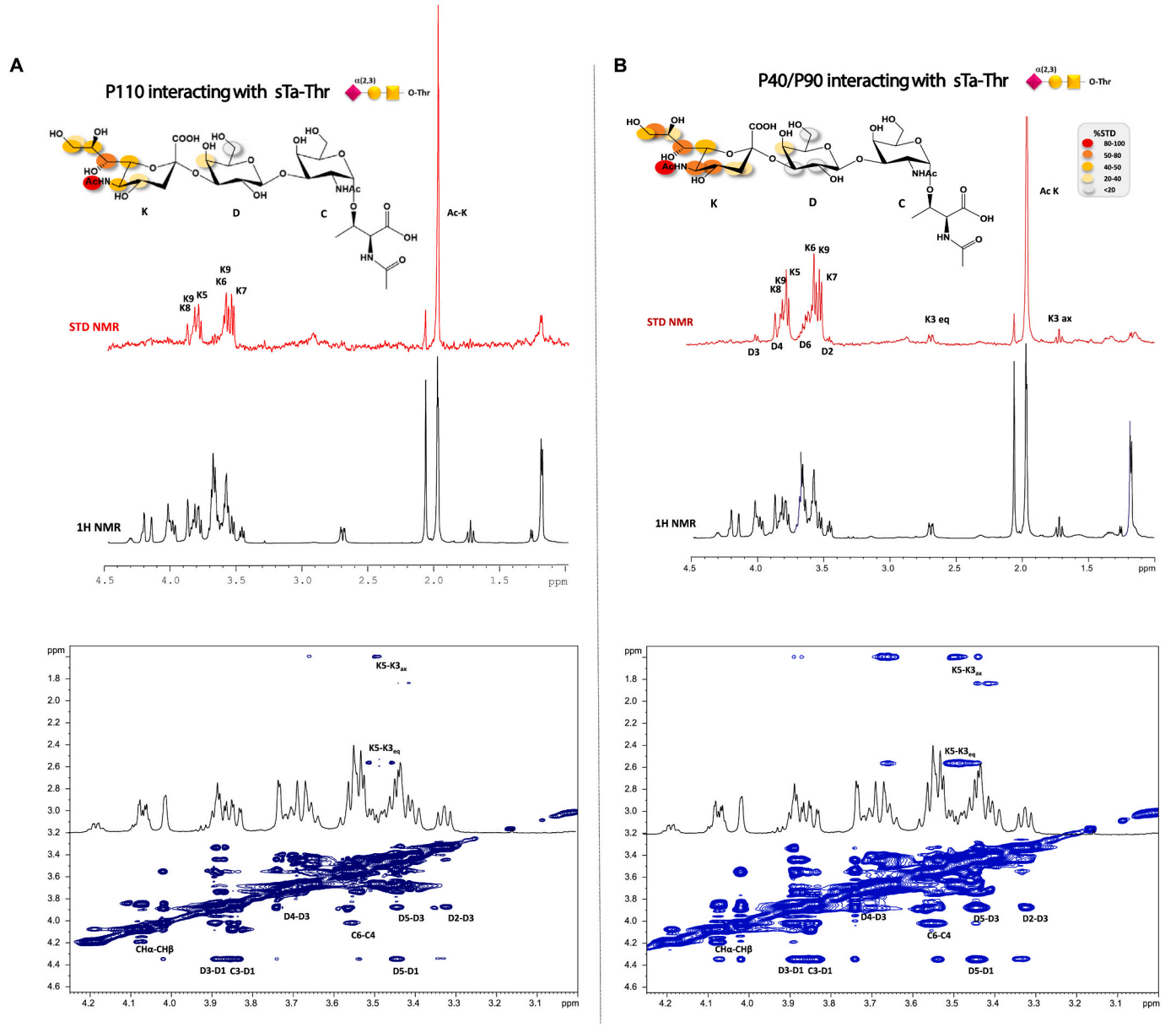

Fig. 7. NMR analysis of sTa-Thr bound to P110 and P40/P90. A) Superimposition of STD-NMR spectrum (red) and the unsaturated reference spectrum (black) of sTa-Thr interacting with P110 and the corresponding ligand epitope map. Are reported. On the bottom, Tr-NOESY spectrum of 1:50 P110-sTa-Thr mixture is reported. B) Superimposition of STD-NMR spectrum (red) and the unsaturated reference spectrum (black) of sTa-Thr interacting with P40/P90 and the corresponding ligand epitope map. On the bottom, Tr-NOESY spectrum of 1:50 P40/P90 -sTa-Thr mixture is reported.

complexes. We provide the first experimental evidence of *Mycoplasma* cytoadhesins binding to *O*-glycans. The study of the interaction between P110 and P40/90 with ad hoc synthesized sTa covalently linked to a threonine (sTa-Thr), representing a natural *O*- glycan exposed on membrane cells, further revealed the ability of these proteins to recognize sialylated glycoproteins, as mucins, with a binding epitope comparable to that observed for their interaction with *N*-glycans. In all predicted complexes, indeed, the sialic acid is the residue that principally contributes to the binding; however, the two cytoadhesins show some differences in the binding sites and shapes. Sialoglycans interacting with P110 always show recurrent H-bonds between the carboxylate group of Neu5Ac and Ser458, the acetamide (NHAc) at position 5 of Neu5Ac and Ser456, and between the proton at position 7 of Neu5Ac with Pro197, in agreement with NMR data since all these ligand moieties exhibited high STD responses. In P40/P90-sialoglycan complexes, Thr632 is involved in the H-bond with carboxyl group of Neu5Ac, the proton at position 7 interacts with Pro235, and the NHAc at position 5 of Neu5Ac makes a H-bond with Leu630. Additionally, hydrophobic amino acids in proximity to the protein binding pocket contribute to stabilize the complexes anchoring the terminal Neu5Ac moiety. Accordingly, a preliminary 3D model of binding between *Mycoplasma* cytoadhesins and longer complex-type *N*-glycans, commonly decorating the host cell surface at mucosal sites, suggests that the binding is mainly governed by polar and hydrophobic interactions with the terminal Neu5Ac moieties, without the involvement in the recognition process of the other sugar units that result to be solvent-exposed.

Thus, we here demonstrate that P110 and P90/P40 can recognize *N*- and *O*-glycans, showing comparable binding epitopes but different conformational aspects. Indeed, while a conformer selection is observed in the complexes with P110, the higher flexibility of a loop close to P40/P90 binding site enables a greater conformational freedom of the ligands interacting with this cytoadhesin.

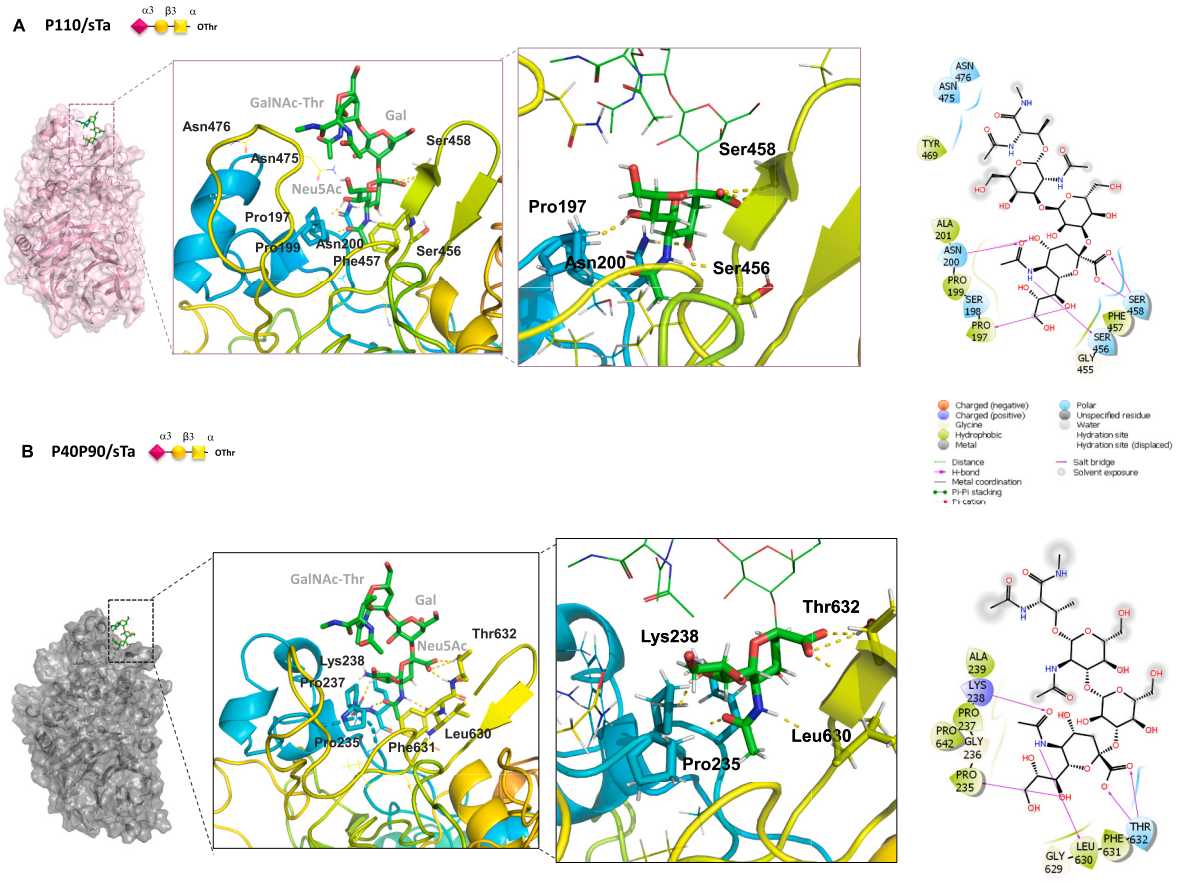

Fig. 8. P110 and P40/P90–sTa-Thr predicted complexes. A) 3D view of the P110-sTa-Thr complex. B) 3D view of the P40/P90-sTa complex. For clarity, a zoom on the Neu5Ac is also reported. The aa of the binding pocket involved in the binding with Neu5Ac are represented as sticks. Two-dimensional plots highlighting the main protein-ligand interactions are also shown. Solid arrows represent hydrogen bonds with the functional groups of the backbone; the other residues in the binding pocket participate in polar and hydrophobic interactions.

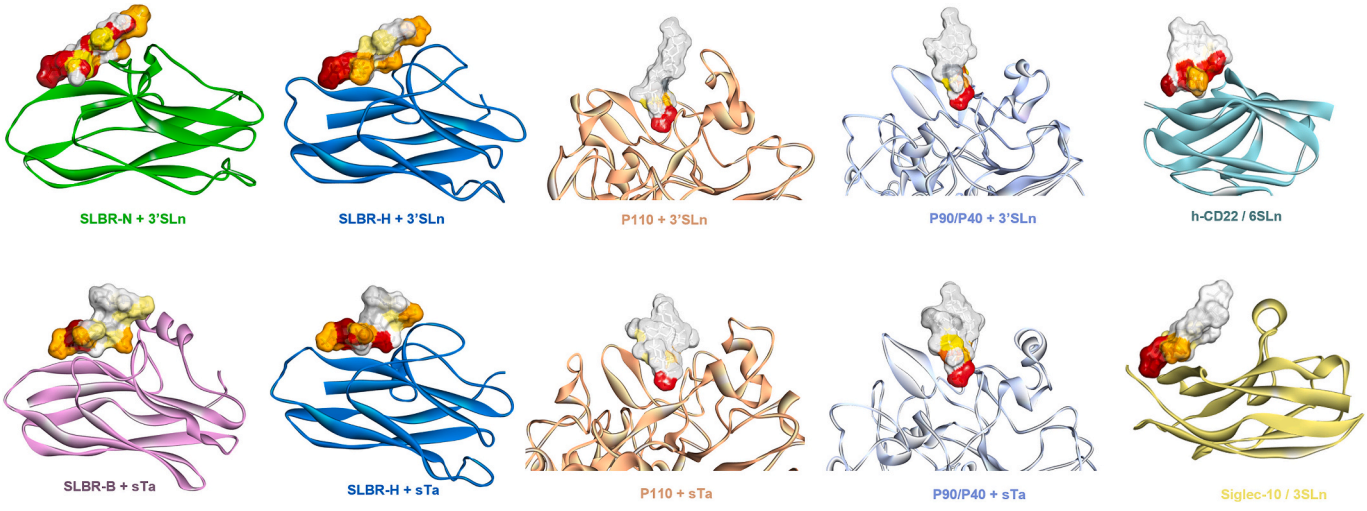

Fig. 9. Comparison of sialoglycans recognition by cytoadhesins with bacterial Siglec-like adhesins and human Siglecs. Predicted models of 3'SLn and/or sTa-Thr bound to streptococcal adhesins, $SLBR_{UB10712}$, $SLBR_{Hsa}$ and $SLBR_{GspB}$, (previously published in ref. [25] and [33]), CD22 and Siglec10 (previously reported in ref. [36] and [28]) and *Mycoplasma* cytoadhesins, P110 and P40/P90 (here explored). In all the predicted complexes the ligand surface is colored according to the STD-derived epitope mapping, highlighting the different binding mode of streptococcal Siglec-like adhesins compared to that of *Mycoplasma* cytoadhesins. The PDB codes of the proteins used for computational analyses of the bound states in the previously published papers [25,33] are 6EFF [50], 6EFD [45], 5IUC [51] and 5VKM [37] for $SLBR_{UB10712}$, $SLBR_{Hsa}$, $SLBR_{GspB}$ and CD22,respectively. Given the crystal structure Siglec-10 had not been solved yet, a predicted model of the protein was built by homology modelling [28].

Notably, the outcomes here reported suggest that the mode of action of *Mycoplasma* cytoadhesins is different from that of other bacterial adhesins, such as streptococcal Siglec-like adhesins, despite a remarkable topological similarity between their sugar binding sites (Fig. 9). We previously indicated that the Siglec-like binding region (SLBR) of adhesins exposed on the surface of *Streptococcus gordonii*, such as $SLBR_{Hsa}$ and $SLBR_{GspB}$ and $SLBR_{UB10712}$, have a wide binding pocket, characterized by the presence of a ΦTRX motif, with the central Thr and Arg residues establishing key H-bonds with the Neu5Ac moiety. Similarly, the glycans' recognition by *Mycoplasma* cytoadhesinsinvolves a crucial H-bond between the carboxylate group of Neu5Ac and a Thr or Ser residue of the protein (Ser458 in P110 and Thr632 in P90/P40). However, crucial flexible loops in streptococcal SLBRs' binding site not only influences their selectivity for Neu5Ac-α-(2-3)-Gal glycosidic linkages, but also permits the recognition of extended ligand epitopes; as showed in Fig. 9, indeed, streptococcal Siglec-like adhesins accommodate the entire sialoglycan moiety via interactions between several amino acids of the binding pocket and different sugar residues besides the terminal Neu5Ac [25,36]. On the contrary, *Mycoplasma* cytoadhesins show a binding mode that involves exclusively the terminal end of sialoglycans, similarly to several mammalian Siglecs (Fig. 9) although the nature of interactions at protein-ligand interface presents some differences. Siglecs preferentially accommodate the terminal Neu5Ac into their binding site via a crucial salt bridge established by the carboxyl group of the sialic acid moiety with the canonical Arg residue located on the F strand. Polar and hydrophobic interactions further contribute to the Neu5Ac recognition process, rarely involving the adjacent sugar units [28,37,38]. *Mycoplasma* cytoadhesins exhibit instead a common Neu5Ac binding motif composed of an extended tripeptide (X-Phe/Tyr-Ser/Thr) [15] exclusively interacting with the terminal sialic acid moiety by relevant polar and hydrophobic contacts.

Moreover, we here hypothesize that *Mycoplasma* adhesins could recognize longer complex *N*-glycans by using a branched binding mode involving both sialic acid residues, located at the termini of the two antennae, in the interaction. NMR experiments on isotopically labelled glycans, together with mutagenesis experiments followed by binding measurements need to be performed to further validate the proposed model of the interaction. Notably, the ability of the serine-rich repeat adhesin $SLBR_{SrpA}$ to bind complex sialoglycans containing two sialic acid residues had previously been hypothesized, thanks to the presence of arginine residues corresponding to both a bacterial and mammalian sialoglycan [39]However, the lack of a crystal structure as well as a model of branched glycans bound to $SLBR_{SrpA}$ hampers the comparison of this binding mode with that of *Mycoplasma* adhesins.

To conclude, our results provide a more comprehensive knowledge of the structural features governing the recognition of sialoglycan ligands by the main cytoadhesins from *M. pneumoniae* and *M. genitalium*, defining the molecular basis of ligand specificity of these bacterial virulence factors. Our analysis provides a critical, atomic-level picture of these interactions, which can be used to identify competitive binding compounds able to selectively inhibit bacterial adherence to host target cells. These insights pave the way for developing innovative strategies to counteract and/or treat bacterial infections based on cytoadherence inhibition.

4. Materials and methods

4.1. Proteins production

For the Ectodomain Region of P110: The region corresponding to the MG_192 gene from *M. genitalium* (strain G37 residues 23–938) was amplified from a synthetic clone, (Genscript) using forward primer P110F and reverse primer P110R. These PCR fragments were subsequently cloned into the pOPINE54 expression vector (gift from Ray Owens, Addgene plasmid #26043) to create a C-terminal Histidine-tagged protein.

The recombinant protein was produced through overnight expression in B834(DE3) cells (Merck) at 20 °C after induction with 1 mM IPTG at an OD600 of 0.6. Cell lysis was carried out in 1× PBS buffer via sonication. Afterward, the cell extract was centrifuged at 20 krpm at 4 °C, and the supernatant was applied to a 5 mL Histrap column (GE Healthcare) equilibrated with 1× PBS as a binding buffer and 1× PBS with 500 mM imidazole as an elution buffer. Soluble aliquots of His6-tagged P110 were pooled and loaded onto a HiLoad Superdex 200 16/60 column (GE Healthcare) in a buffer containing 50 mM Tris pH 7.4 and 150 mM NaCl [15].

For the Ectodomain Region of P40/P90: The ectodomain region of P40/P90 (23–1114) was amplified from the synthetic clone of the MPN_142 gene (GenScript) from *M. pneumoniae* using forward primer P40P90_F and reverse primer P40P90_R. The PCR fragment was subsequently cloned into the pOPINE expression vector. The recombinant protein was obtained after expression in B834(DE3) cells (Merck) induced with 0.8 mM IPTG at 22 °C overnight. The cell pellets were lysed in a buffer containing 40 mM Imidazole and 30 mM Tris-HCl at pH 7.4 (binding buffer) and then centrifuged at 20,000 RPM at 4 °C. The supernatant was loaded onto a HisTrap 5 mL column (GE Healthcare) and eluted with a buffer containing 400 mM imidazole. Soluble aliquots were concentrated and loaded onto a Superdex 200 GL 10/300 column (GE Healthcare) pre-equilibrated with 20 mM Tris·HCl buffer at pH 7.4 and 150 mM NaCl [16].

4.2. Ligands

The 3'sialylactosamine (3'SLn) and 6'sialylactosamine (6'SLn) were purchased from Tokyo Chemical Industry Co., Ltd. The sialyl-T-antigen linked to the threonine (sTa-Thr) was chemically synthesized as previously reported [40]. The sugar moiety of sialyl-T-antigen (without threonine) was purchased from Biosynth. The biantennary N-glycans were provided from GlyTech, Inc. [41].

4.3. Fluorescence spectroscopy

Steady-state fluorescence experiments were performed on a Fluoromax-4 spectrofluorometer from Horiba Scientific (Edison, USA). All the measurements were acquired at a controlled temperature of 25 °C, the excitation wavelength was selected at 280 nm and the emission spectra collected between 290 and 500 nm. The slits were set to 5 nm for both the excitation and emission monochromators. All the spectra were recorded after an equilibration time of 3 min in a 1 cm path-length quartz cuvette, under constant stirring.

A fixed concentration of both P110 and P40/P90 proteins was selected at 0.07 μM in 1.2 mL PBS buffer (pH 7.4) and titrated by adding small amounts of each ligand 3'SLn, 6'SLn, sTa-Thr and sTa in the range from 0 to 6.5 μM (1–100 μL of a ligand stock solution of 84 μM). In these conditions, it was possible to observe the quenching of protein fluorescence in presence of the three different ligands; in particular, no ligand emission interference was observed.

Data analysis was performed using the software Origin 8.1. Specifically, the binding curves were obtained by plotting F/F_{max} values versus ligand concentrations, where F and F_{max} are fluorescence intensities in presence and in absence of the ligands, respectively. The binding constants (K_b) were determined by non-linear regression with One Site-Specific Binding model, as described in detail in Ribeiro et al., 2008; Oliva et al., 2019; Forgione et al., 2020 [27,42,43].

4.4. NMR analysis

The NMR experiments were recorded on a Bruker AVANCE NEO 600 MHz equipped with a cryo probe. Data acquisition and processing were performed with TOPSPIN 4.1.1 software. All NMR samples were prepared in 50 mM deuterate phosphate buffer (NaCl 140 mM, Na_2HPO_4 10 mM, KCl 3 mM, pH 7.4 and the [D4] (trimethylsilyl)propionic acid,

sodium salt (TSP, 10 μM) was used as internal reference to calibrate all the spectra. The chemical shifts of the glycan ligands were assigned by 1H, COSY, TOCSY, NOESY and HSQC experiments [44].

Tr-NOESY analysis. Homonuclear 2D $^{1}H—^{1}H$ NOESY experiments were carried out by using data sets of 2048 × 512 points and mixing times of 200 ms. Protein to ligand ratios from 1:20 to 1:50 were used [45].

STD NMR analysis. All the NMR spectra were acquired in the same conditions for P110 and P40/P90, using protein concentrations of 20 μM and ligand concentrations of 1 mM (protein:ligand ratio of 1:50) and temperature of 298 K. Control experiments with the ligands and proteins in the absence of the protein and the ligand, respectively, were performed to optimize STD NMR parameters [46]. STD NMR experiments were acquired with 64 K data points and zero-filled prior to processing and a number of scans of 72 and 128. The protein resonances were selectively irradiated using 40 Gauss pulses with a length of 50 ms, setting the off-resonance pulse frequency at 40 ppm and the on-resonance pulse at 0 and 7.5 ppm. All STD experiments were performed by using the sequence "stddiffesgp" with an excitation sculpting with gradient pulses (esgp) for the suppression of water signals. A saturation time of 2 s were used for all STD-NMR experiments. By using these conditions, no STD signals were observed in the control STD NMR spectra of the ligands alone.

The epitope mapping of ligands was achieved by the calculation of the ratio $(I_0 - I_{sat})/I_0$, where $(I_0 - I_{sat})$ is the intensity of the signal in the STD NMR spectrum and I_0 is the peak intensity referred to the unsaturated reference spectrum (off-resonance). The highest STD signal was set to 100 % and all the other STD were normalized to this value.

4.5. MM and MD simulations

Molecular dynamics calculations of 100 ns on ligands alone and bound to the proteins P110 and P40/P90 were carried out by using the AMBER 18 software package [47] in explicit water using the following forcefields: Glycam06j-1 for the glycans and FF14SB for the proteins. All the oligosaccharides were built up and minimized by using Maestro package and the carbohydrate builder utility of the glycam website (www.glycam.com) [48], and then the torsional angles were set to the values obtained through the molecular mechanics calculations.

First, the ligands were manually docked into the proteins binding pocket according to the published structures (PDB used: 6RUT and 6TLZ for P110 and P40/P90 respectively). Before the MD simulation, the complexes were minimized using Sander tools. The molecules were neutralized by adding Na^+ ions and then hydrated with an octahedral box of TIP3P water of the proper size and the remote interactions were calculated using a cut-off of 10 Å applying *tleap* module of the AMBER package. The MD calculations were performed by using the PMEMD. CUDA implementation within AMBER 18 package. Periodic boundary conditions were applied, as well as the smooth particle mesh Ewald method to represent the electrostatic interactions, with a grid space of 1 Å. A restriction to the protein, which was gradually released, was applied and the system was minimized. Furthermore, the whole system was slowly heated from 0 to 300 K using a weak restrain on the solute and then, the system was equilibrated at 300 K using constant pressure and removing the restrains on the solute. Concerning the complexes of P110 and P40/P90 with sTa-Thr, the value of the peptide dihedral angle (O-CB-CA-N) was restrained approximately at 60°.

Coordinates were obtained to acquire 10,000 structures representing the progression of the dynamics. The trajectories were assessed using the ptraj module in AMBER 18 and the MD results were visualized using the VMD program [49]. A cluster analysis of the MD trajectory was applied based on ligand RMSD, employing the K-means algorithm integrated into the *ptraj* module. The representative structures of the most populated clusters were selected to depict the complexes interactions. Multiple representative poses were chosen for each MD simulation. The identification of hydrogen bonds was computed using the CPPTAJ module within AMBER 18, defining a hydrogen bond as forming between an acceptor heavy atom (A), a donor hydrogen atom (H), and a donor heavy atom (D). The distance cut-off was chosen at 3 Å, and the A-H-D angle cut-off was set to 135°. The frequency of protein-ligand bonds formed during the dynamics was reported with a 5 Å cut-off.

CRediT authorship contribution statement

Angela Marseglia: Writing – review & editing, Writing – original draft, Formal analysis, Data curation. **Maria Concetta Forgione:** Writing – review & editing, Writing – original draft, Formal analysis, Data curation. **Marina Marcos-Silva:** Writing – review & editing, Formal analysis. **Cristina Di Carluccio:** Writing – review & editing, Formal analysis. **Yoshiyuki Manabe:** Writing – review & editing, Formal analysis. **David Vizarraga:** Writing – review & editing, Formal analysis. **Ferran Nieto-Fabregat:** Writing – review & editing, Formal analysis, Data curation. **Maria Pia Lenza:** Writing – review & editing, Formal analysis. **Koichi Fukase:** Writing – review & editing, Formal analysis. **Antonio Molinaro:** Writing – review & editing, Conceptualization. **Oscar Q. Pich:** Writing – review & editing, Formal analysis, Conceptualization. **David Aparicio:** Writing – review & editing, Formal analysis, Conceptualization. **Alba Silipo:** Writing – review & editing, Conceptualization. **Roberta Marchetti:** Writing – review & editing, Writing – original draft, Supervision, Funding acquisition, Formal analysis, Data curation, Conceptualization.

Declaration of competing interest

The authors declare that they have no known competing financial interests or personal relationships that could have appeared to influence the work reported in this paper.

Data availability

Data will be made available on request.

Acknowledgements

This project has received funding from the European Research Council (ERC) under the European Union's Horizon 2020 research and innovation program under grant agreement No 851356 to R.M. FSE, PON Ricerca e Innovazione Azione I.1 "Dottorati Innovativi con caratterizzazione Industriale" is acknowledged for funding the PhD grant to A.M. A.S. and R.M. acknowledge PNRR, Missione 4 – Componente 2 – NextGenerationEU - Partenariato Esteso INF-ACT - One Health Basic and Translational Research Actions Addressing Unmet Needs on Emerging Infectious Diseas-es MUR: PE00000007. F.N-F. acknowledges Italian MUR, PRIN 2020, Project SEA-WAVE 2020BKK3W9.

Appendix A. Supplementary data

Supplementary data to this article can be found online at https://doi.org/10.1016/j.ijbiomac.2024.135277.

References

[1] J. Pizarro-Cerdá, P. Cossart, Bacterial adhesion and entry into host cells, Cell 124 (4) (2006) 715–727.
[2] W. Loveless, T. Feizi, Sialo-oligosaccharide receptors for Mycoplasma pneumoniae and related oligosaccharides of poly-N-Acetyllactosamine series are polarized at the cilia and apical-Microvillar domains of the ciliated cells in human bronchial epithelium, Infect. Immun. 57 (4) (1989) 1285–1289.
[3] Williams, C.R.; Chen, L.; Sheppard, E.S.; Chopra, P.; Locklin, J.; Boons, G-J.; Krause DC. (2020) Distinct Mycoplasma pneumoniae interactions with sulfated and sialylated receptors. Infect. Immun. 88: e00392-20.
[4] L. Qin, Y. Chen, X. You, Subversion of the immune response by human pathogenic mycoplasmas, Front. Microbiol. 10 (1934) (2019) 1–12.
[5] K.B. Waites, D.F. Talkington, Mycoplasma pneumoniae and its role as a human pathogen, Clin. Microbiol. Rev. 17 (4) (2004) 697–728.

[6] T.P. Atkinson, M.F. Balish, K.B. Waites, Epidemiology, clinical manifestations, pathogenesis and laboratory detection of Mycoplasma pneumoniae infections, FEMS Microbiol. Rev. 32 (6) (2008) 956–973.

[7] D.F. Talkington, K.B. Waites, S.B. Schwartz, R.E. Besser, Emerging from obscurity: understanding pulmonary and extrapulmonary syndromes, pathogenesis, and epidemiology of human Mycoplasma pneumoniae infections, Emerg. Infect. Dis. (2001) 57–84.

[8] S. Kashyap, M. Sarkar, Mycoplasma pneumonia: clinical features and management, Lung India 27 (2) (2010) 75–85.

[9] W. Yueyue, X. Feichen, X. Yixuan, L. Lu, C. Yiwen, Y. Xiaoxing, Pathogenicity and virulence of Mycoplasma genitalium: unraveling Ariadne's thread, Virulence 13 (1) (2022) 1161–1183.

[10] C.L. McGowin, C. Anderson-Smits, Mycoplasma genitalium: an emerging cause of sexually transmitted disease in women, PLoS Pathog. 7 (5) (2011) e1001324.

[11] Ona, S.; Molina, R. L.; Diouf, K. (2016) Mycoplasma genitalium: an overlooked sexually transmitted pathogen in women? *Infect dis Obstet Gynecol*, 4513089.

[12] C.P. Smullin, H. Green, R. Peters, D. Nyemba, Y. Qayiya, L. Myer, J. Klausner, D. Joseph Davey, Prevalence and incidence of Mycoplasma genitalium in a cohort of HIV-infected and HIV-uninfected pregnant women in Cape Town, South Africa. Sex Transm Infect 96 (7) (2020) 501–508.

[13] D. Nakane, T. Kenri, L. Matsuo, M. Miyata, Systematic structural analyses of attachment organelle in Mycoplasma pneumoniae, PLoS Pathog. 11 (12) (2015) e1005299.

[14] P.C. Hu, R.M. Cole, Y.S. Huang, J.A. Graham, D.E. Gardner, A.M. Collier, W. A. Clyde, Mycoplasma pneumoniae infection: role of a surface protein in the attachment organelle, Science 216 (1982) 313–315.

[15] D. Aparicio, S. Torres-Puig, M. Ratera, E. Querol, J. Piñol, O.Q. Pich, I. Fita, Mycoplasma genitalium adhesin P110 binds sialic-acid human receptors, Nat. Commun. 9 (1), 4471 (2018) 1–11.

[16] D. Vizarraga, A. Kawamoto, U. Matsumoto, R. Illanes, R. Pérez-Luque, J. Martín, R. Mazzolini, P. Bierge, O.Q. Pich, M. Espasa, I. Sanfeliu, J. Esperalba, M. Fernández-Huerta, M.P. Scheffer, J. Pinyol, A.S. Frangakis, M. Lluch-Senar, S. Mori, K. Shibayama, T. Kenri, T. Kato, K. Namba, I. Fita, M. Miyata, D. Aparicio, Immunodominant proteins P1 and P40/P90 from human pathogen Mycoplasma pneumoniae, Nat. Commun. 11 (1) (2020).

[17] D. Aparicio, M.P. Scheffer, M. Marcos-Silva, D. Vizarraga, L. Sprankel, M. Ratera, M.S. Weber, A. Seybert, S. Torres-Puig, L. Gonzalez-Gonzalez, J. Reitz, E. Querol, J. Piñol, O.Q. Pich, I. Fita, A.S. Frangakis, Structure and mechanism of the nap adhesion complex from the human pathogen Mycoplasma genitalium, Nat. Commun. 11 (1) (2020) 2877.

[18] D. Vizarraga, S. Torres-Puig, D. Aparicio, O.Q. Pich, The Sialoglycan binding Adhesins of Mycoplasma genitalium and Mycoplasma pneumoniae, Trends Microbiol. 29 (6) (2021) 477–481.

[19] G. Taylor, Sialidases: structures, biological significance and therapeutic potential, Curr. Opin. Struct. Biol. 6 (1996) 830–837.

[20] A. Gaskell, S. Crennell, G. Taylor, The three domains of a bacterial sialidase: a beta-propeller, an immunoglobulin module and a galactose-binding jelly-roll, Structure 3 (11) (1995) 1197–1205.

[21] N.M. Varki, A. Varki, Diversity in cell surface sialic acid presentations: implications for biology and disease, Lab. Invest. 87 (9) (2007) 851–857.

[22] D.D. Roberts, L.D. Olson, M.F. Barile, V. Ginsburg, H.C. Krivan, Sialic acid-dependent adhesion of Mycoplasma pneumoniae to purified glycoproteins, J. Biol. Chem. 264 (16) (1989) 9289–9293.

[23] D.F. Talkington, K.B. Waites, S.B. Schwartz, R.E. Besser, Emerging from obscurity: understanding pulmonary and extrapulmonary syndromes, pathogenesis, and epidemiology of human Mycoplasma pneumoniae infections, in: W.M. Scheld, W. A. Craig, J.M. Hughes (Eds.), Emerging Infections 5, ASM Press, Washington, DC, 2001, pp. 57–84.

[24] L. Sprankel, M.P. Scheffer, S. Manger, U.H. Ermel, A.S. Frangakis, Cryo-electron tomography reveals the binding and release states of the major adhesion complex from Mycoplasma genitalium, PLoS Pathog. 19 (11) (2023) e1011761.

[25] E. Gianchecchi, A. Arena, A. Fierabracci, Sialic acid-Siglec Axis in human immune regulation, involvement in autoimmunity and Cancer and potential therapeutic treatments, Int. J. Mol. Sci. 22 (11) (2021) 5774.

[26] C. Di Carluccio, R.E. Forgione, A. Bosso, S. Yokoyama, Y. Manabe, E. Pizzo, A. Molinaro, K. Fukase, M. Fragai, B.A. Bensing, R. Marchetti, A. Silipo, Molecular recognition of sialoglycans by streptococcal Siglec-like adhesins: toward the shape of specific inhibitors, RSC Chem Biol 2 (6) (2021) 1618–1630.

[27] O.A. Chernova, E.S. Medvedeva, A.A. Mouzykantov, N.B. Baranova, V.M. Chernov, Mycoplasmas and their antibiotic resistance: the problems and prospects in controlling infections, Acta Nat. 8 (2) (2016) 24–34.

[28] C. Di Carluccio, M.C. Forgione, S. Martini, F. Berti, A. Molinaro, R. Marchetti, A. Silipo, Investigation of protein-ligand complexes by ligand-based NMR methods, Carbohydr. Res. 503 (2021) 108313.

[29] R.E. Forgione, C. Di Carluccio, J. Guzmán-Caldentey, R. Gaglione, F. Battista, F. Chiodo, Y. Manabe, A. Arciello, P. Del Vecchio, K. Fukase, A. Molinaro, S. Martín-Santamaría, P.R. Crocker, R. Marchetti, A. Silipo, Unveiling molecular recognition of Sialoglycans by human Siglec-10, iScience 23 (6) (2020) 101231.

[30] L. Poppe, R. Stuike-Prill, B. Meyer, H. van Halbeek, The solution conformation of Sialyl-$\alpha(2\rightarrow6)$-lactose studied by modern NMR techniques and Monte Carlo simulations, J. Biomol. NMR 2 (2) (1992) 109–136.

[31] T. Walther, R. Karamanska, R.W. Chan, M.C. Chan, N. Jia, G. Air, C. Hopton, M. P. Wong, A. Dell, J.S. Malik Peiris, S.M. Haslam, J.M. Nicholls, Glycomic analysis of human respiratory tract tissues and correlation with influenza virus infection, PLoS Pathog. 9 (3) (2013) e1003223.

[32] T. Kasai, D. Nakane, H. Ishida, H. Ando, M. Kiso, M. Miyata, Role of binding in Mycoplasma mobile and Mycoplasma pneumoniae gliding analyzed through inhibition by synthesized sialylated compounds, J. Bacteriol. 195 (3) (2013) 429–435.

[33] R.J. Manchee, D. Taylor-Robinson, Utilization of neuraminic acid receptors by mycoplasmas, J. Bacteriol. 98 (1969) 914–919.

[34] O. Sobeslavsky, B. Prescott, R.M. Chanock, Adsorption of Mycoplasma pneumoniae to neuraminic acid receptors of various cells and possible role in virulence, J. Bacteriol. 96 (1968) 695–705.

[35] R.A. Alvarez, M.W. Blaylock, J.B. Baseman, Surface localized glyceraldehyde-3-phosphate dehydrogenase of Mycoplasma genitalium binds mucin, Mol. Microbiol. 48 (5) (2003) 1417–1425.

[36] Di Carluccio, C.; Cerofolini, L.; Moreira, M.; Rosu, F.; Padilla-Cortés, L.; Gheorghita, G.R.; Xu, Z.; Santra, A.; Yu, H.; Yokoyama, S.; Gray, T. E.; St. Laurent, C. D.; Manabe, Y.; Chen, X.; Fukase, K.; Macauley, M. S.; Molinaro, A.; Li, T.; Bensing, B. A.; Marchetti, R,; Gabelica, V.; Fragai, M.; Silipo A. (2024) Molecular insights into O-linked Sialoglycans recognition by the Siglec-like SLBR-N $_{(SLBRUB10712)}$ of Streptococcus gordonii. ACS Cent. Sci., 10, 2, 447–459.

[37] R.E. Forgione, F.F. Nieto, C. Di Carluccio, F. Milanesi, M. Fruscella, F. Papi, C. Nativi, A. Molinaro, P. Palladino, S. Scarano, M. Minunni, M. Montefiori, M. Civera, S. Sattin, O. Francesconi, R. Marchetti, A. Silipo, Conformationally constrained Sialyl analogues as new potential binders of h-CD22, Chembiochem: a European journal of chemical biology 23 (10) (2022) e202200076.

[38] C. Di Carluccio, R. E. Forgione, A. Molinaro, P. R. Crocker, R. Marchetti, and A. Silipo, in Carbohydrate Chemistry: Chemical and Biological Approaches, Volume 44, ed. A. Pilar Rauter, T. K. Lindhorst, and Y. Queneau, The Royal Society of Chemistry, 2020, vol. 44, pp. 31–55.

[39] L.V. Loukachevitch, B.A. Bensing, H. Yu, J. Zeng, X. Chen, P.M. Sullam, T. M. Iverson, Structures of the streptococcus sanguinis SrpA binding region with human Sialoglycans suggest features of the physiological ligand, Biochemistry 55 (2016) 5927–5937.

[40] J.B. Schwarz, S.D. Kuduk, X.-T. Chen, D. Sames, P.W. Glunz, S.J. Danishefsky, A broadly applicable method for the efficient synthesis of α-O-linked Glycopeptides and clustered sialic acid residues, J. Am. Chem. Soc. 121 (12) (1999) 2662–2673.

[41] Y. Kajihara, Y. Suzuki, N. Yamamoto, K. Sasaki, T. Sakakibara, L.R. Juneja, Prompt chemoenzymatic synthesis of diverse complex-type oligosaccharides and its application to the solid-phase synthesis of a glycopeptide with Asn-linked sialyl-undeca- and asialo-nonasaccharides, J. Chem. 10 (4) (2004) 971–985.

[42] M.M. Ribeiro, H.G. Franquelim, M.A. Castanho, A.S. Veiga, Molecular interaction studies of peptides using steady-state fluorescence intensity. Static (de) quenching revisited, J. Pept. Sci. 14 (4) (2008) 401–406.

[43] R. Oliva, F. Battista, S. Cozzolino, E. Notomista, R. Winter, P. Del Vecchio, L. Petraccone, Encapsulating properties of sulfobutylether-β-cyclodextrin toward a thrombin-derived antimicrobial peptide, J. Therm. Anal. Calorim. 138 (2019) 3249–3256.

[44] I. Speciale, A. Notaro, P. Garcia-Vello, F. Di Lorenzo, S. Armiento, A. Molinaro, R. Marchetti, A. Silipo, C. De Castro, Liquid-state NMR spectroscopy for complex carbohydrate structural analysis: a hitchhiker's guide, Carbohydr. Polym. 277 (2022) 118885.

[45] M.J. Angulo, B. Langpap, A. Blume, T. Biet, B. Meyer, N.R. Krishna, H. Peters, M. M. Palcic, T. Peters, Blood group B galactosyltransferase: insights into substrate binding from NMR experiments, J. Am. Chem. Soc. 128 (41) (2006) 13529–13538.

[46] B. Mayer, B. Meyer, Group epitope mapping by saturation transfer difference NMR to identify segments of a ligand in direct contact with a protein receptor, J. Am. Chem. Soc. 123 (25) (2001) 6108–6117.

[47] D.A. Case, I.Y. Ben-Shalom, S.R. Brozell, D.S. Cerutti, T.E. Cheatham, V.W. D. Cruzeiro, T.A. Darden, R.E. Duke, D. Ghoreishi, M.K. Gilson, H. Gohlke, A. W. Goetz, D. Greene, R. Harris, N. Homeyer, Y. Huang, S. Izadi, A. Kovalenko, T. Kurtzman, T.S. Lee, S. LeGrand, P. Li, C. Lin, J. Liu, T. Luchko, R. Luo, D. J. Mermelstein, K.M. Merz, Y. Miao, G. Monard, C. Nguyen, H. Nguyen, I. Omelyan, A. Onufriev, F. Pan, R. Qi, D.R. Roe, A. Roitberg, C. Sagui, S. Schott-Verdugo, J. Shen, C.L. Simmerling, J. Smith, R. SalomonFerrer, J. Swails, R.C. Walker, J. Wang, H. Wei, R.M. Wolf, X. Wu, L. Xiao, M. York, P.A. Kollman, AMBER 2018, University of California, San Francisco, 2018.

[48] Group, W. GLYCAM Web. http://glycam.org.

[49] W. Humphrey, A. Dalke, K. Schulten, VMD: visual molecular dynamics, J. Mol. Graph. 14 (1), 33-8 (1996) 27–28.

[50] B.A. Bensing, H.E. Stubbs, R. Agarwal, I. Yamakawa, K. Luong, K. Solakyildirim, H. Yu, A. Hadadianpour, M.A. Castro, K.P. Fialkowski, K.M. Morrison, Z. Wawrzak, X. Chen, C.B. Lebrilla, J. Baudry, J.C. Smith, P.M. Sullam, T.M. Iverson, Origins of glycan selectivity in streptococcal Siglec-like adhesins suggest mechanisms of receptor adaptation, Nat. Commun. 13 (2022) 2753.

[51] T.M. Pyburn, B.A. Bensing, Y.Q. Xiong, B.J. Melancon, T.M. Tomasiak, N.J. Ward, V. Yankovskaya, K.M. Oliver, G. Cecchini, G.A. Sulikowski, M.J. Tyska, P. M. Sullam, T.M. Iverson, A structural model for binding of the serine-rich repeat adhesin GspB to host carbohydrate receptors, PLoS Pathog. 7 (2011) e1002112.